Journal of Hazardous Materials 168 (2009) 1140–1146

Contents lists available at ScienceDirect

Journal of Hazardous Materials

journal homepage: www.elsevier.com/locate/jhazmat

Characteristics and defluoridation performance of granular activated carbons coated with manganese oxides

Yue Ma [a], Shu-Guang Wang [a,*], Maohong Fan [b], Wen-Xin Gong [a], Bao-Yu Gao [a]

[a] School of Environmental Science and Engineering, Shandong University, 27 Shanda Nanlu, Jinan 250100, China
[b] School of Energy Resources & Department of Chemical & Petroleum Engineering, University of Wyoming, Laramie, WY 82071, USA

ARTICLE INFO

Article history:
Received 3 December 2008
Received in revised form 25 February 2009
Accepted 26 February 2009
Available online 13 March 2009

Keywords:
Defluoridation
Adsorption
Manganese-oxide-coated granular activated carbon (GAC-MnO_2)
Adsorption kinetics
Non-linear chi-square test

ABSTRACT

Using a redox process, granular activated carbon (GAC) was coated with manganese oxides to enhance its ability to adsorb fluoride from an aqueous solution. Compared with plain GAC, the fluoride adsorption capacity of this new adsorbent was improved and at least three times greater than that of uncoated GAC. The surface characteristics of coated GAC were observed with scanning electron microscopy. The surface area of the new adsorbent was calculated using the Brunauer–Emmett–Teller method. X-ray diffraction revealed that manganese oxides are amorphous. X-ray photoelectron spectroscopy demonstrated that manganese existed primarily in the oxidation state +IV. Kinetic and equilibrium adsorption data showed that the adsorption process follows the pseudo-second order kinetic and Freundlich equation models. The sorption data also indicated that the removal of fluoride by adsorption is a highly complex process, involving both boundary layer diffusion and intra-particle diffusion. The pH value of solution influences fluoride removal, and the optimum equilibrium pH value of fluoride adsorption is 3.0.

1. Introduction

According to World Health Organization (WHO) guidelines, the optimum fluoride level in drinking water is between 0.5 and 1.0 mg/L [1]. As an essential micronutrient, fluoride is beneficial for the calcification of dental enamel and bone formation. However, excess intake is very harmful to human beings. The long-term consumption of water with fluoride concentrations exceeding WHO guidelines not only causes dental and skeletal fluorosis, but may also lead to mutations in the consumer's deoxyribonucleic acid (DNA) [2]. China is one country where fluorosis is endemic to many areas. Since the 1970s, fluorosis has been widespread in many provinces and autonomous regions, including Shanxi, Fujian, Shandong, Ningxia, and Inner Mongolia, among others. In some areas, the prevalence of dental fluorosis in children is nearly 100%, with skeletal fluorosis in adults as high as 70–80% [3].

Current methods used to remove fluoride from water typically include chemical precipitation, ion exchange, adsorption, membrane processes, Donnan dialysis and electrodialysis [4,5]. Each of the technology has been found to be limited, since the membrane processes often have high operational costs and the chemical precipitation may produce large amount of sludge. Among these methods, adsorption is still one of the most extensively used methods for defluoridation because of its ease of operation and cost effectiveness.

Activated carbon is generally recognized as an effective adsorbent due to its high porosity, large surface area, and high catalytic activity, and is currently widely used for the removal of organic compounds in drinking water [6]. Used in a column process, activated carbon can eliminate separation problems and minimize sludge production. However, activated carbon has a relatively small adsorption capacity as well as an affinity for inorganic pollutants [7]. To enhance adsorption efficacy, the modification of existing adsorbents with suitable chemicals has been investigated with promising results, suggesting that the new adsorbents might remove fluoride from aqueous solutions effectively [4,8]. For example, Ramos et al. [9] increased the maximum fluoride uptake capacity of activated carbon by impregnating it with aluminum. However, this synthetic process is time-consuming, taking more than 6 days to complete. And while recent research has demonstrated that material coated with manganese oxide for the removal of fluoride can enhance treatment capacity and efficiency [5], studies on activated carbon coated with manganese oxide for fluoride removal have not yet been reported.

This study investigates the defluoridation potential of a new adsorbent, manganese-oxide-coated granular activated carbon (GAC-MnO_2). The adsorbent was prepared by coating activated carbon with manganese oxide through a redox process. The modified activated carbon was characterized using a variety of techniques and removal tests were carried out to understand its

* Corresponding author. Tel.: +86 531 88362802; fax: +86 531 88364513.
E-mail address: wsg@sdu.edu.cn (S.-G. Wang).

0304-3894/$ – see front matter © 2009 Elsevier B.V. All rights reserved.
doi:10.1016/j.jhazmat.2009.02.145

adsorption behaviors, including kinetics, sorption isotherm, and pH-dependent performance.

2. Materials and methods

2.1. Preparation of adsorbents

Granular activated carbon (GAC) from plant shell was purchased from the GuangCheng Chemical Plant in Tianjin. All other chemical reagents used were analytical grade and contained negligible fluoride impurities. Deionized water (pH = 5.8 ± 0.2) was used throughout the study.

Activated carbon was crushed and sieved within a specific particle size range (0.45–0.9 mm), and then immersed for 12 h in a 37.5% solution of hydrochloric acid to reduce ash content. After acid treatment, it was washed repeatedly to reach neutrality and dried in a 105 °C oven for 24 h.

A composite of manganese oxide with GAC was prepared by chemical precipitation of manganese oxide from $KMnO_4$ and $MnCl_2$ water solutions in the presence of GAC. 5 g GAC was immersed in 50 mL solutions of $MnCl_2$ at various concentrations. To enable better incorporation into the cavities of GAC, the suspension was vigorously stirred at room temperature for 6 h. pH of the suspension was 3.3 ± 0.1 at the beginning of mingling and there was no pH control during the process of stirring. Large amounts of $KMnO_4$ were subsequently added to the suspension under continuous stirring to oxidate Mn^{2+}, immediately turning the solution dark brown, which indicated the formation and precipitation of MnO_2, i.e.:

$$3Mn^{2+} + 2MnO_4^- + 2H_2O = 5MnO_2\downarrow + 4H^+ \quad (1)$$

Finally, the suspension was filtered, washed several times with distilled water, and dried once again at 105 °C. Activated carbon thus prepared is denominated "manganese-oxide-coated granular activated carbon."

2.2. Properties of adsorbents

The adsorbents were characterized using several techniques. The surface morphology of the plain GAC and GAC-MnO_2 samples was visualized using a Hitachi S-4800 scanning electron microscope (SEM). The specific surface area was measured by nitrogen adsorption/desorption at −196 °C using the Brunauer–Emmett–Teller (BET) method with a Quantachrome QUADRASORB SI surface area and pore size analyzer. Mineralogy of the GAC-MnO_2 was characterized by X-ray diffraction (XRD) using a Rigaku D/max RA X-ray powder diffractometer. The XRD data were matched with standard JCPDS data. GAC and GAC-MnO_2 samples were also analyzed by Fourier Transform Infrared Spectroscopy (FTIR) using a Thermo Nicolet Spectrometer, and X-ray photoelectron spectroscopy (XPS) using a Perkin-Elmer PHI 5300 X-ray Photoelectron Spectrometer. The pH_{PZC} (pH of point of zero charge) of GAC-MnO_2 was determined by batch equilibrium [10].

2.3. Batch adsorption experiments

A stock solution of fluoride was prepared by dissolving sodium fluoride in deionized water. Fluoride-bearing solutions were prepared by diluting the stock solution to specific concentrations. All experiments were conducted at room temperature (28 °C). Adjustments for pH were done using 0.1 M HCl or 0.1 M NaOH.

Batch adsorption experiments were conducted to examine time-dependent sorption behavior and the effects of temperature and solution pH on adsorption performance. Sorption kinetic experiments were conducted using 5 g of GAC-MnO_2 in 1 L of fluoride solution at various concentrations (viz. 10, 20, and 30 mg/L) in Teflon bottles. Under continuous stirring using a magnetic stir bar, samples were collected utilizing a 0.45 μm Millipore filter at predetermined time intervals. The filtrates were measured with a fluoride ions-selective electrode, using a total ionic strength adjustment buffer (TISAB) solution to eliminate any effects from the interference of complex ions. Fluoride uptake was calculated by performing a mass balance using the following equation:

$$q_t = \frac{(C_0 - C_t)V}{m} \quad (2)$$

where q_t is the amount of adsorbed fluoride at time t (mg/g); V is the volume of solution (L); C_0 (mg/L) and C_t (mg/L) are initial and residual fluoride concentrations at time t, respectively; and m is the mass of adsorbent (g).

Equilibrium adsorption isotherms were defined by agitating 0.5 g GAC-MnO_2 with 100 mL of a desired fluoride solution at various temperatures (25, 40 and 55 °C) in a shaking machine. At a predetermined time interval (3 h), the concentration of residual fluoride was measured immediately after it was filtered.

In the pH experiment, initial solution pH was adjusted to the desired value range of about 2–11. 0.5 g of GAC-MnO_2 was added into each vial along with 100 mL of solution and agitated for 3 h with an orbital shaker. Finally, fluoride concentration and pH were analyzed.

3. Results and discussion

3.1. Optimization and characterization

Coating MnO_2 on GAC can not only increase the number of active sites that play an important role in the sorption process but also affect the micro-porous structure of GAC. Thus it is necessary to determine the optimal amount of MnO_2 to apply to the GAC. The modified samples obtained at various concentrations (0.2, 0.3, 0.4, 0.8 M) of $MnCl_2$ solution were prepared and investigated in the adsorption of fluoride from an aqueous solution. In the adsorption experiments, 0.5 g GAC-MnO_2 with different amounts of MnO_2 was introduced into Teflon bottles to which 100 mL of fluoride solution containing varying concentrations (3–35 mg/L) at pH 5.2 was added. After being stirred for 3 h, the concentrations of fluoride in the solution were measured.

As shown in Fig. 1, the adsorption capacity of the modified carbon increases with the increase of the quantity of the MnO_2 coated on GAC. The adsorption capacities of the coated GAC obtained with a 0.3 M $MnCl_2$ solution under different conditions are higher than

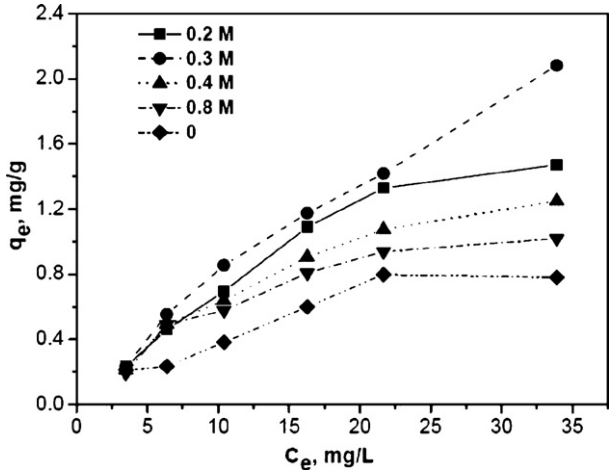

Fig. 1. Effect of MnO_2 coating amount on fluoride adsorption (adsorbent dose = 5.0 g/L, pH = 5.2 ± 0.2, and T = 28 ± 1 °C).

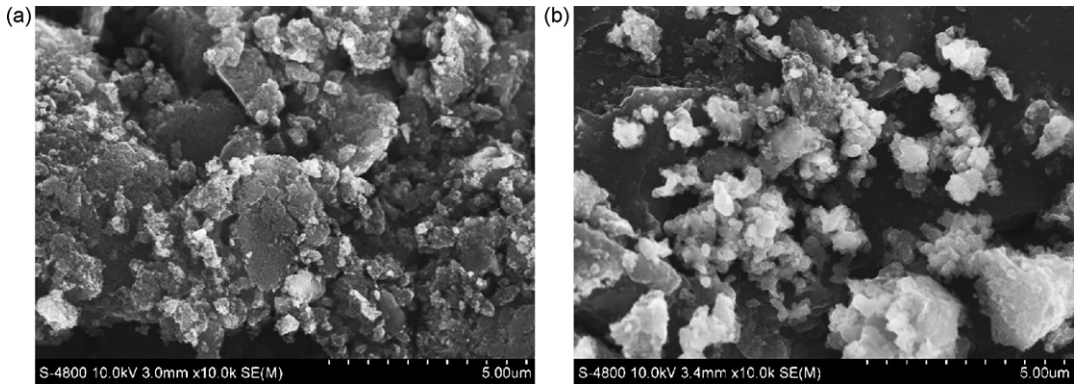

Fig. 2. Micrographs of plain GAC (a) and GAC-MnO_2 (b).

those achieved with other coated GAC, and at least three times greater than those of uncoated GAC. Therefore, this GAC-MnO_2 specimen was chosen as the sample in the following characterization and batch adsorption experiment. The amount of manganese on the surface of the GAC-MnO_2, measured through acid digestion analysis was approximately 40.48 mg Mn/g GAC-MnO_2.

SEM enables the direct observation of any microstructural changes on the surface of activated carbon that might have occurred due to the modification. The SEM photographs in Fig. 2 were taken at 10,000× magnification to observe the surface morphology of plain GAC and MnO_2-coated GAC. The SEM image of pristine GAC in Fig. 2a shows that it has a relatively uniform surface with small cracks and micro-pores. By contrast, GAC-MnO_2 (Fig. 2b) evidenced a comparatively rougher surface, and it could also be observed that a large number of small particles were formed on the surface of the carbon during the modification process. In order to better characterize the composite particles, the modified sample was analyzed by the energy dispersive X-ray spectrometer system (EDAX). One of those particles was characterized with EDAX and shown in Fig. 3. The EDAX spectrum shows that C, Mn, and O are the major elements present on the surface of the characterized particles. The strengths of peaks in the EDAX spectra are proportional to the concentrations of the corresponding elements and indicate that Mn exists in the form of MnO_2 on the surface of the GAC.

The oxide coatings affected not only the morphology but also the surface area and porosity of the GAC. The surface area of the GAC-MnO_2 is 914.17 m^2/g—slightly higher than that of the plain GAC (850.60 m^2/g). After surface coating, pore specific volume increased from 0.509 to 0.803 cm^3/g, which may result from the increase in both inner and surface porosity after adding manganese oxides.

To better understand surface properties, the pH_{PZC} of GAC-MnO_2 was measured, revealing a value of approximately 3.0. The XRD spectrum of the sample (data not shown) reveals that the MnO_2 on GAC-MnO_2 is in an amorphous phase, as there is no visible peak detected.

FTIR spectra are employed to understand the formation of composites. Fig. 4 shows the FTIR spectra of GAC and GAC-MnO_2. The broad, strong band in the 3400–3600 cm^{-1} range may be due to the O–H bending vibrations, which show the presence of surface hydroxyl groups and physically absorbed water [11–13]. The strong adsorption bands at 1500–1650 cm^{-1} (centered at 1543 and 1622 cm^{-1}) are indicated both for the double bond (C=C) vibrations in an aromatic system and the highly conjugated C–O stretching vibration bands [11,14]. Additionally, the weak intensity of the 1622 cm^{-1} peak indicates that the activated carbon contains a small amount of the carboxyl group [13]. The sharp peak at 1118 cm^{-1} could be due to C–O stretching vibration, which is consistent with

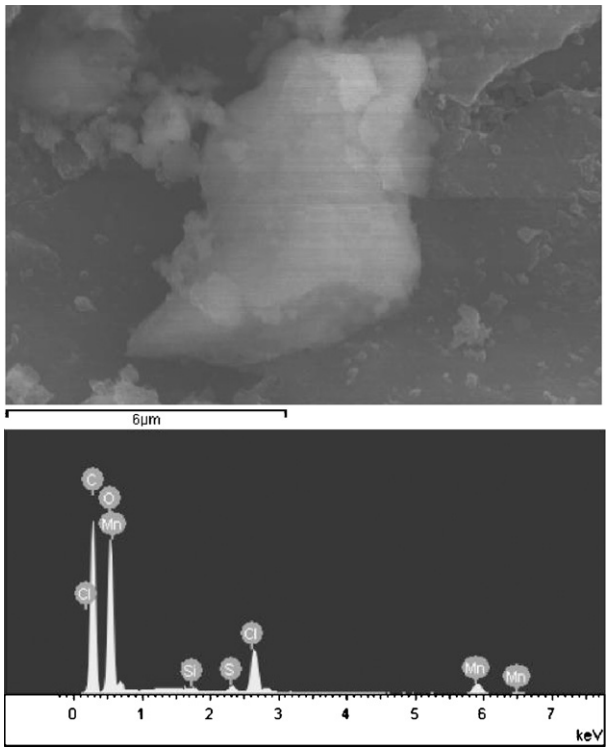

Fig. 3. EDAX spectrum of GAC-MnO_2.

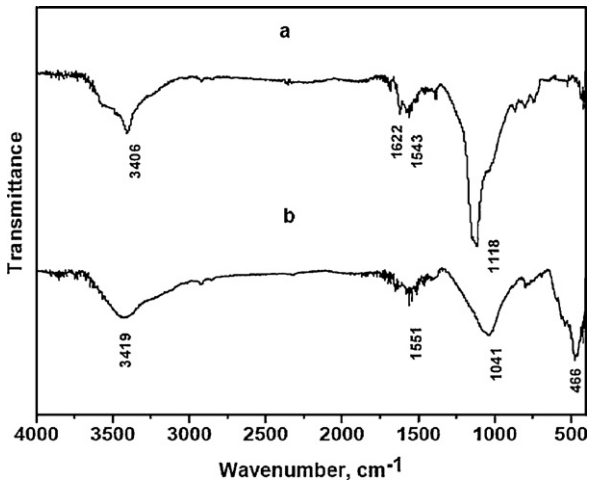

Fig. 4. FTIR spectra of GAC (a) and GAC-MnO_2 (b).

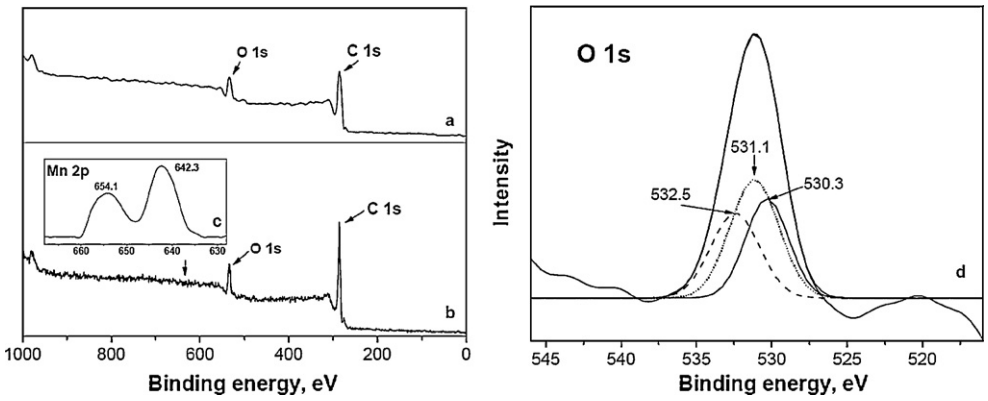

Fig. 5. XPS spectra of: pristine GAC (a), GAC-MnO_2 (b), Mn 2p peak of GAC-MnO_2 (c), O 1s peak of GAC-MnO_2 (d).

the peak at 3400–3600 cm^{-1}, verifying the existence of hydroxyl [15].

Compared with the FTIR spectrum of GAC, an obvious change of the spectrum for GAC-MnO_2 (Fig. 4b) lies in the appearance of a new band at 466 cm^{-1}, which may be attributed to Mn–O bond stretching [16]. This also indicates that MnO_2 has been successfully coated on GAC. The peak in the range of 3400–3600 cm^{-1} shown in Fig. 4a broadened at 3419 cm^{-1} in Fig. 4b, indicating that O–H on the surface of GAC shifted significantly due to its modification with MnO_2. Moreover, surface modification of GAC narrowed the peak at 1551 cm^{-1} in the 1500–1650 cm^{-1} region, which might be caused by the moieties of C=C, a well-known red-shifted phenomenon on oxygen-rich surfaces with diminution of the C=O peak centered at 1622 cm^{-1}. The sharp peak of C–O stretching vibration changes to a broader peak centered at 1041 cm^{-1}, which is likely due to the overlapping of C–O stretching and Mn–OH vibration [17].

XPS is helpful for further determining the elements present and their chemical state (i.e. valence). Considering the spectra as a whole (Fig. 5a and b), the ratio of O 1s to C 1s peaks demonstrates a remarkable change, possibly due to the change of the surface functional groups revealed by FTIR analysis. Fig. 5c shows the Mn 2p spectrum of the GAC-MnO_2 before adsorption. The binding energies (BEs) of the Mn $2p_{1/2}$ and the Mn $2p_{3/2}$ are determined to be 654.07 and 642.30 eV, respectively. The BEs of Mn $2p_{3/2}$ peaks are often used to estimate the valence of manganese, and a BE of 642 eV is generally assigned to Mn (IV) [18].

The O 1s peak of GAC-MnO_2 can be decomposed into three components (Fig. 5d): the lowest energy contribution (530.32 eV), assigned to oxygen involved in Mn–O–Mn bonds [17,18]; the second (531.2 eV), attributed mainly to newborn hydroxides bound to manganese [17,18]; and the third (532.6 eV), attributed to oxygen making single bonds with hydrogen or carbon (C–O–H of alcohol and carboxyl) [19].

From FTIR and XPS analyses, the hydroxyl and carboxyl groups on the activated carbon are involved in the modification process. The corresponding change in the molecular structure during the preparation of the new adsorbent may be proposed as shown in Eq. (3).

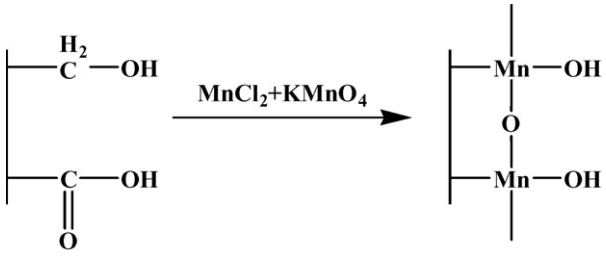

(3)

3.2. Adsorption kinetics

Fig. 6 shows the effect of agitation time and initial concentration on the adsorption of fluoride. It can be demonstrated that most sorption took place in the first 30 min and that the uptake of fluoride ions reached saturation in 180 min. Therefore, 180 min was fixed as the optimum contact time for other experiments. It is also clear from Fig. 6 that the amount of uptake is highly dependent on the initial concentration of fluoride ions in the solution. Equilibrium uptake (q_e) increased along with the increase of the initial concentrations of fluoride ions, thus demonstrating that the initial concentration is a driving force to overcome the resistance of mass transfer between the soluble and solid phases.

The rate of sorption onto a solid surface is determined by many parameters, e.g. the initial concentrations of the solute, the structural properties of the sorbent, the interaction between the solute and the active sites of the sorbent, etc. The kinetics of sorption describes the solute uptake rate, which in turn governs the residence time of sorption reaction, the knowledge of which is critical in designing appropriate adsorption technologies. Thus, kinetic data of fluoride sorption onto GAC-MnO_2 were studied with pseudo-first and pseudo-second order kinetic models.

The pseudo-first order equation is given as:

$$\ln(q_e - q_t) = \ln\ q_e - k_1 t \tag{4}$$

The pseudo-second order equation is expressed as:

$$\frac{t}{q_t} = \frac{1}{k_2 q_e^2} + \frac{1}{q_e} t \tag{5}$$

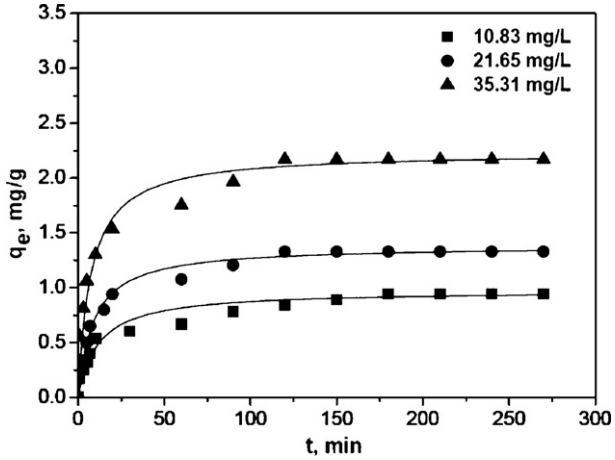

Fig. 6. Adsorption kinetic curves of fluoride at various initial concentrations (adsorbent dose = 5.0 g/L, pH = 5.2 ± 0.2, T = 28 ± 1 °C).

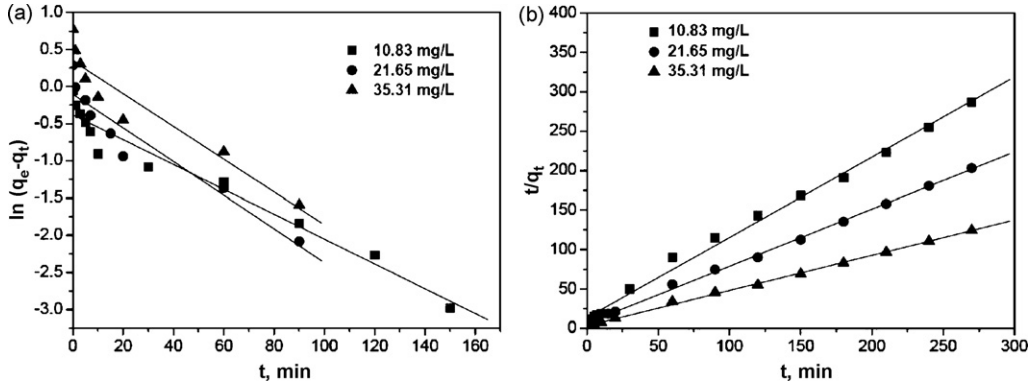

Fig. 7. Linearization of fluoride adsorption kinetics onto GAC-MnO_2 (a) pseudo-first order rate; (b) pseudo-second order rate.

Both kinetic models were applied to the experimental data (Fig. 7). The results, presented in Table 1, clearly show that the adsorption of fluoride onto the GAC-MnO_2 obeys the pseudo-second order equation ($R^2 \geq 0.995$). Also, the adsorption capacities calculated by the model are close to those results obtained from experiments. In contrast, for q_e, the values estimated from the pseudo-first order kinetic model give significantly different values compared to experimental values, and the coefficients of determination (R^2) are also found to be fairly lower. These results suggest that experimental data for the adsorption kinetics of fluoride ions on the GAC-MnO_2 better fit the pseudo-second order kinetic model, and that chemical sorption involving valency forces may limit the sharing or exchange of electrons between anions and adsorbent [20]. The values of the pseudo-second order rate constant, k_2, quoted in Table 1, decrease with the increase of the initial fluoride concentration.

Theoretically, the adsorption kinetics of fluoride onto solid particles is controlled by different mechanisms [21]: (a) external mass transfer, (b) adsorption of fluoride ions onto particle surfaces, and (c) intra-particle diffusion. Eqs. (4) and (5) cannot identify the diffusion mechanism. Sorption kinetic data were further processed to determine whether intra-particle diffusion is rate limiting and also to find the rate parameter for intra-particle diffusion (K_P), which is determined using the following equation [22]:

$$q_t = K_P t^{0.5} + C \tag{6}$$

By the plot of q_t versus $t^{0.5}$, multilinearities are observed in Fig. 8, indicating that three steps took place. In the first step, the sharper linear portion (dash lines) is attributed to the boundary layer diffusion. The second linear portion (solid lines) describes the gradual adsorption stage, in which intra-particle diffusion is rate-controlled. The third portion (dotted lines) is attributed to the final equilibrium stage, during which intra-particle diffusion started to slow down due to extremely low solute concentrations in the solution [22].

If intra-particle diffusion is the only rate-determining step, the second portion could be extended to pass through the origin; if not, the boundary layer diffusion controlled the adsorption to some degree. It could be concluded that there are three processes that

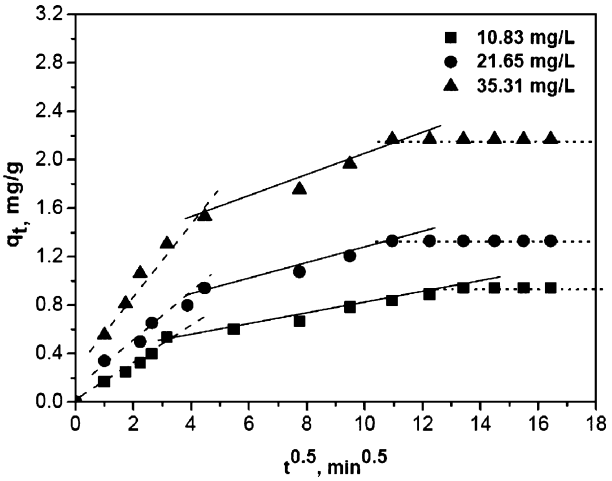

Fig. 8. Plots of the intra-particle diffusion kinetics equation for adsorption of fluoride ions onto GAC-MnO_2 with different initial concentrations of adsorbate.

controlled the rate of molecular adsorption, but only one was rate limiting over any particular time range [22,23]. The solid line (linear) portions of the curves fail to pass through the origin (Fig. 8), indicating that the mechanism of fluoride removal on GAC-MnO_2 is complex and that both surface adsorption as well as intra-particle diffusion contributes to the rate-determining step.

3.3. Adsorption isotherm

The most commonly applied isotherms in solid/liquid systems are the theoretical equilibrium isotherms, viz. Langmuir, Freundlich and Redlich–Peterson.

The Langmuir equation is applicable to homogeneous sorption where the sorption of each sorbate molecule onto the surface has equal sorption activation energy. The Langmuir model can be described by the following equation:

$$q_e = \frac{q_m K_a C_e}{1 + K_a C_e} \tag{7}$$

Table 1
Adsorption rate constant obtained from pseudo-first order model and pseudo-second order model for various initial concentrations of fluoride.

Initial fluoride concentration (mg/L)	Pseudo-first order			Pseudo-second order		
	k_1 (min^{-1})	q_e (mg/g)	R^2	k_2 (g/(mg min))	q_e (mg/g)	R^2
10.83	0.018	0.68	0.959	0.088	0.97	0.995
21.65	0.023	0.90	0.910	0.080	1.38	0.999
35.31	0.022	1.41	0.896	0.061	2.24	0.999

Table 2
Comparison of coefficient of determination, R^2 and non-linear chi-square test analysis, χ^2.

Temperature (°C)	Langmuir		Freundlich		Redlich–Peterson	
	R^2	χ^2	R^2	χ^2	R^2	χ^2
25	0.336	4.1679	0.995	0.0068	0.996	0.0091
40	0.105	6.7855	0.981	0.004	0.998	0.0053
55	0.762	5.5606	0.987	0.0116	0.996	0.0155

It can also be represented by the following linearized expression:

$$\frac{C_e}{q_e} = \frac{1}{q_m} C_e + \frac{1}{K_a q_m} \quad (8)$$

The most important multisided adsorption isotherm for heterogeneous surfaces is the Freundlich adsorption isotherm, characterized by the heterogeneity factor $1/n$. The Freundlich model is described by:

$$q_e = K_F C_e^{1/n} \quad (9)$$

and is represented by the linearized equation:

$$\ln\ q_e = \ln K_F + \frac{1}{n} \ln C_e \quad (10)$$

The Redlich–Peterson isotherm is an empirical isotherm incorporating three parameters. It combines elements from both the Langmuir and Freundlich equations, and the mechanism of adsorption is a hybrid that does not follow ideal monolayer adsorption:

$$q_e = \frac{AC_e}{1 + BC_e^{\beta}} \quad (11)$$

It can also be represented using a linear form:

$$\ln\left(A\frac{C_e}{q_e} - 1\right) = \beta \ln(C_e) + \ln(B) \quad (12)$$

The three linear isotherms for the adsorption of fluoride onto GAC-MnO_2, at different temperatures were fitted to the experimental data and the results of their linear regression were used to determine the best fitting model among them. The coefficients of determination (R^2) are listed in Table 2. It can be seen that the Freundlich (Fig. 9) and Redlich–Peterson models show significantly higher correlations ($R^2 \geq 0.98$) than the Langmuir models. Furthermore, the values of exponent β calculated from Redlich–Peterson plots are found to be close to 0 (data not shown), which biases this model towards the Freundlich model [24]. However, the transformation of non-linear isotherm equations to linear forms implicitly alters their error structure and may also violate the error variance and normality assumptions of standard least squares. Therefore, it is necessary to analyze the data set using the non-linear chi-square test (χ^2) in order to validate the most appropriate isotherm for the sorption system. The results of the non-linear chi-square test analysis are also presented in Table 2. Correspondingly, the χ^2 test also shows tendencies similar to R^2. Therefore, the Freundlich model is selected as the most appropriate model for the adsorption of fluoride onto GAC-MnO_2. Because the Freundlich model is based on the assumption of adsorption onto heterogeneous surfaces, it is also evident that the surface of GAC-MnO_2 is heterogeneous. This may result from the large number of different functional groups on an activated carbon surface as well as the various adsorbent–adsorbate interactions.

3.4. Effect of initial pH

Generally, pH is an important factor affecting the defluoridation at water–adsorbent interfaces. Fig. 10 presents the fluoride uptake and pH of the solution after adsorption at different initial pH values, ranging from 2 to 11. Fluoride adsorption was found to vary with respect to initial solution pH. It was observed that the amount of fluoride uptake increased with initial pH up to 8, and that maximum uptake occurred at a pH value between initial pH values of 8 and 9. It also indicates the removal of fluoride is maximum at equilibrium pH 3.0, which would be expected of fluoride-containing industrial wastewater [25]. In the acid pH range pH < 3, adsorption is expected to take place mainly by anion exchange, as shown in Eq. (13) [26]:

$$\text{GAC-MnO}_2 \cdot x\text{H}_2\text{O}_{(\text{solid})} + \text{F}^-_{(\text{aq})} \rightarrow \text{GAC-MnO}_2 \cdot (x-1)\text{H}_2\text{O} \cdot \text{H}^+\text{F}^-_{(\text{solid})} + \text{OH}^- \quad (13)$$

GAC-MnO_2 has a pH_{PZC} of 3.0, which means that in the pH range of 3–11 the surface of the adsorbent presents a net negative charge. GAC-MnO_2 functions as a cation-exchanger and adsorbs sodium ions present in solution releasing protons [26]. This process can be

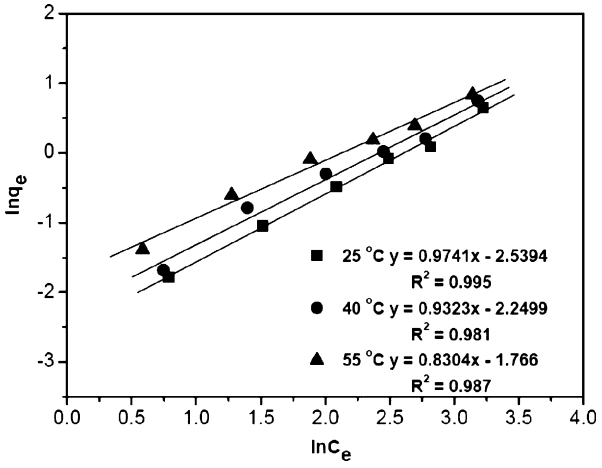

Fig. 9. Linearization of Freundlich isotherm for removal of fluoride (adsorbent dose = 5.0 g/L, pH = 5.2 ± 0.2).

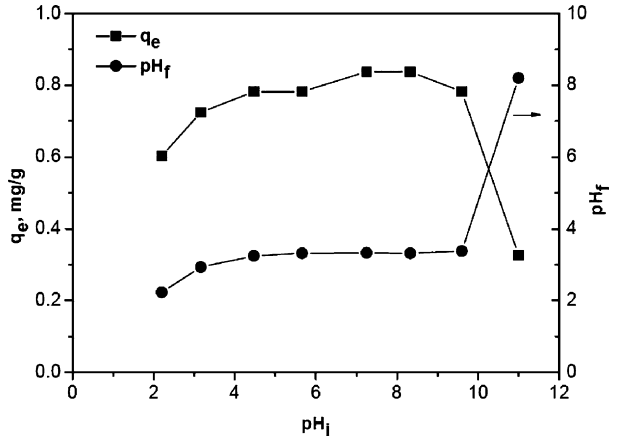

Fig. 10. Effect of initial pH on fluoride adsorption (adsorbent dose = 5.0 g/L, an initial concentration = 10 mg/L, $T = 28 \pm 1$ °C).

described as follows:

$$\text{GAC-MnO}_2\cdot x\text{H}_2\text{O}_{(\text{solid})} + \text{Na}^+{}_{(\text{aq})} + \text{F}^-{}_{(\text{aq})} \rightarrow \text{GAC-MnO}_2\cdot(x-1)\text{H}_2\text{O}\cdot\text{OH}^-\text{Na}^+\text{F}^-{}_{(\text{solid})} + \text{H}^+ \quad (14)$$

The final pH close to 3 after adsorption at the initial pH in the range of 3–9 was most probably caused by the low pH nature of the GAC-MnO_2. When pH of the solution approached the pH_{PZC} of GAC-MnO_2, the aforementioned reaction would no longer occur. Furthermore, when the adsorbent was exposed to an extreme basic condition, the MnO_2 dissolved, resulting in a poor adsorption capacity when initial pH was above 11.

4. Conclusions

In this study, manganese-oxide-coated granular activated carbon was prepared and its fluoride adsorption capacity was evaluated. The following conclusions could be drawn from the above studies.

MnO_2 could be coated on activated carbon as small particles through a redox reaction. The defluoridation capacity of activated carbon was enhanced by MnO_2 coating. The on GAC-MnO_2 is a non-stoichiometric, amorphous phase.

The processes of modification can alter the physical and chemical structure of GAC, causing an apparent increase in its specific surface area. The functional groups on the GAC surface are also modified.

Fluoride adsorption onto GAC-MnO_2 follows the pseudo-second order kinetics pattern. Both surface adsorption and intra-particle diffusion contribute to the rate-determining step, and the adsorption equilibrium data agree with Freundlich isotherms in the tested concentration and temperature ranges.

The modified carbon is capable of maintaining a high fluoride adsorption capacity over an acidic pH range. Therefore, it is useful in treating polluted water at low pH.

Acknowledgments

We appreciate the support provided by Projects in the National Science & Technology Pillar Program, China (2006BAJ08B05-2).

References

[1] WHO (World Health Organization), Guidelines for Drinking Water Quality, World Health Organization, Geneva, 2006.
[2] T. Tsutsui, N. Suzuki, M. Ohmori, H. Maizumi, Cytotoxicity, chromosome aberrations and unscheduled DNA synthesis in cultured human diploid fibroblasts induced by sodium fluoride, Mutat. Res. 139 (1984) 193–198.
[3] H. Wang, G.X. Teng, Brief instruction of the prevention of endemic fluorosis, Chin. J. Clin. Rehabil. 44 (2006) 222–225.
[4] S.S. Tripathy, J. Bersillon, K. Gopal, Removal of fluoride from drinking water by adsorption onto alum-impregnated activated alumina, Sep. Purif. Technol. 50 (2006) 310–317.
[5] S.M. Maliyekkal, A.K. Sharma, L. Philip, Manganese-oxide-coated alumina: a promising sorbent for defluoridation of water, Water Res. 40 (2006) 3497–3506.
[6] L. Li, P.A. Quinlivan, D.R.U. Knappe, Effects of activated carbon surface chemistry and pore structure on the adsorption of organic contaminants from aqueous solution, Carbon 40 (2002) 2085–2100.
[7] D. Mugisidi, A. Ranaldo, J.W. Soedarsono, M. Hikam, Modification of activated carbon using sodium acetate and its regeneration using sodium hydroxide for the adsorption of copper from aqueous solution, Carbon 45 (2007) 1081–1084.
[8] Y.M. Zhou, C.X. Yu, Y. Shan, Adsorption of fluoride from aqueous solution on La^{3+}-impregnated cross-linked gelatin, Sep. Purif. Technol. 36 (2004) 89–94.
[9] R.L. Ramos, J. Ovalle-Turrubiartes, M.A. Sanchez-Castillo, Adsorption of fluoride from aqueous solution on aluminum-impregnated carbon, Carbon 37 (1999) 609–617.
[10] B.M. Babić, S.k. Milonjić, M.J. Polovina, B.V. Kaludierović, Point of zero charge and intrinsic equilibrium constants of activated carbon cloth, Carbon 37 (1999) 477–481.
[11] S.H. Park, S. McClain, Z.R. Tian, S.L. Suib, C. Karwacki, Surface and bulk measurements of metals deposited on activated carbon, Chem. Mater. 9 (1997) 176–183.
[12] J.P. Chen, S.N. Wu, Acid/base-treated activated carbons: characterization of functional groups and metal adsorptive properties, Langmuir 20 (2004) 2233–2242.
[13] L.J. Kennedy, J.J. Vijaya, G. Sekaran, K. Kayalvizhi, Equilibrium, kinetic and thermodynamic studies on the adsorption of m-cresol onto micro- and mesoporous carbon, J. Hazard. Mater. 149 (2007) 134–143.
[14] M. Pakuła, M. Walczyk, S. Biniak, A. Świątkowski, Electrochemical and FTIR studies of the mutual influence of lead(II) or iron(III) and phenol on their adsorption from aqueous acid solution by modified activated carbons, Chemosphere 69 (2007) 209–219.
[15] S.B. Deng, Y.P. Ting, Polyethylenimine-modified fungal biomass as a high-capacity biosorbent for Cr (VI) anions: sorption capacity and uptake mechanisms, Environ. Sci. Technol. 39 (2005) 8490–8496.
[16] S.K. Samantaray, K. Parida, Modified TiO_2–SiO_2 mixed oxides. 1. Effect of manganese concentration and activation temperature towards catalytic combustion of volatile organic compounds, Appl. Catal. B: Environ. 57 (2005) 83–91.
[17] B.J. Aronson, C.F. Blanfordand, A. Stein, Synthesis, characterization, and ion-exchange properties of zinc and magnesium manganese oxides confined within MCM-41 channels, J. Phys. Chem. B 104 (2000) 449–459.
[18] S. Ardizzone, C.L. Bianchi, D. Tirelli, Surface reactivity of α-Mn_2O_3 powders in aqueous suspensions, J. Electroanal. Chem. 425 (1997) 19–23.
[19] F. Ahimou, C.J.P. Boonaert, Y. Adriaensen, P. Jacques, P. Thonart, M. Paquot, P.G. Rouxhet, XPS analysis of chemical functions at the surface of *Bacillus subtilis*, J. Colloid Interface Sci. 309 (2007) 49–55.
[20] Y.S. Ho, G. McKay, Pseudo-second order model for sorption processes, Process Biochem. 34 (1999) 451–465.
[21] X. Fan, D.J. Parker, M.D. Smith, Adsorption kinetics of fluoride on low cost materials, Water Res. 37 (2003) 4929–4937.
[22] Y. Önal, C. Akmil-Başar, C. Sarıcı-Özdemir, Elucidation of the naproxen sodium adsorption onto activated carbon prepared from waste apricot: kinetic, equilibrium and thermodynamic characterization, J. Hazard. Mater. 148 (2007) 727–734.
[23] S. Ghorai, K.K. Pant, Equilibrium, kinetics and breakthrough studies for adsorption of fluoride on activated alumina, Sep. Purif. Technol. 42 (2005) 265–271.
[24] O. Redlich, D.L. Peterson, A useful adsorption isotherm, J. Phys. Chem. 63 (1959) 1024–1026.
[25] A. Eskandarpour, M.S. Onyango, A. Ochieng, S. Asai, Removal of fluoride ions from aqueous solution at low ph using schwertmannite, J. Hazard. Mater. 152 (2008) 571–579.
[26] S. Dey, S. Goswami, U.C. Ghosh, Hydrous ferric oxide (HFO)—a scavenger for fluoride from contaminated water, Water Air Soil Pollut. 158 (2004) 311–323.